Boron-doped superlattices and Bragg mirrors in diamond

Alexandre Fiori, Jessica Bousquet, David Eon, Franck Omnès, E Bellet-Amalric, Etienne Bustarret

Boron-doped superlattices and Bragg mirrors in diamond

A. Fiori,[1,2,3] J. Bousquet,[1,2] D. Eon,[1,2] F. Omnès,[1,2] E. Bellet-Amalric,[1,4] and E. Bustarret[1,2,a)]
[1]University of Grenoble Alpes, Inst. NEEL, 38042 Grenoble, France
[2]CNRS, Inst. NEEL, 25 rue des Martyrs, 38042 Grenoble, France
[3]National Institute for Materials Science, 1-1 Namiki, Tsukuba, Ibaraki 305-0044, Japan
[4]CEA-Grenoble, INAC/SP2M, 17 rue des Martyrs, 38054 Grenoble, France

(Received 1 August 2014; accepted 20 August 2014; published online 27 August 2014)

A periodic modulation of the boron doping level of single crystal diamond multilayers over more than three orders of magnitude during epitaxial growth by microwave plasma-enhanced chemical vapor deposition is shown to yield Bragg mirrors in the visible. The thicknesses and doping level of the individual layers were controlled by *in situ* spectroscopic ellipsometry, enabling to tune the reflectance peak to the wavelength range of diamond color centers, such as NV^0 or NV^-. The crystalline quality, periodicity, and sharpness of the doping transitions in these doping superlattices over tens of periods were confirmed by high resolution X-ray diffraction. © *2014 AIP Publishing LLC*.
[http://dx.doi.org/10.1063/1.4894376]

To make the most of the impressive single photon emission properties of diamond color centers, such as the nitrogen-vacancy (NV) or silicon-vacancy (SiV) complexes, it is of paramount importance to enhance the photon production rate as well as the collection efficiency of the emitted photons. Unfortunately, the strategies based on Bragg mirrors which have been so successful in delivering high quality monolithic optical cavities in the field of compound semiconductors could not be applied to diamond, both because of the lack of diamond-based alloys and of the standing challenges of diamond heteroepitaxy. Single crystal diamond films of high quality may so far only be grown by homoepitaxy on diamond substrates, so that the refractive index contrast required for any multilayer photonic device is lacking. Worse, because of the high index of diamond in the visible ($\approx$2.4), the light emitted from a given color center will most likely leak into the substrate because of the high internal reflection coefficient at the diamond/air interface. Some solutions have been proposed: beside diamond nanoparticles, the most popular (but still under development) use either plasma-etched nanowires[1–3] or solid-state immersion lenses fabricated with a focused ion beam[4,5] (FIB). Impressive early demonstrations of 3D micromachining by a combination of ion irradiation, FIB, and wet etching[6] are being more rarely followed up. In this work, we propose to consider diamond heavily boron-doped at concentrations [B] larger than a few $10^{20}\,cm^{-3}$ as a metallic diamond (p^+) alloy. The difference in refractive index (index contrast) between p^+ single crystal epilayers and non-intentionally doped ($[B] < 10^{17}\,cm^{-3}$) diamond (i) layers increases with wavelength[7–9] (around 10% at 600 nm and 20% at 800 nm), along with the absorption coefficient related to the plasmon oscillations present in p^+ diamond. Despite these limitations, we shall demonstrate in the following that it is possible to make Bragg mirrors out of diamond by alternating the growth at two different doping levels, and to tune their periodic refraction properties to the emission wavelengths of a specific color center. Aiming at the upper limit of the range of interest, around 850 nm (there is, for example, a Ni-related center emitting[10] at 880 nm), where the index contrast is highest, a first p^+ip^+i periodic homoepitaxial stack (SL1) was grown on a type IIa optical grade (001)-oriented diamond substrate. Then, we fabricated other mirrors reflecting visible light, closer to the emission range of the negatively-charged NV^- or neutral NV^0 centers.[1–5] These have a zero-phonon emission line at 638 and 575 nm, respectively, but their room temperature spectra involve also sizable phonon-related broad bands at longer wavelengths, a drawback that is not shared by the less phonon-coupled SiV^- center emitting at 737 nm. Two other superlattices (SL2 and SL3) were grown for the purpose on type Ib and type IIa diamond substrates, respectively.

In order to obtain such samples, a standing TE_{10} microwave was generated in a rectangular horizontal waveguide, and a vertical quartz tube was positioned at a maximum of the electric field. A diamond coated substrate holder was held at mid-height of the waveguide of this microwave plasma-assisted chemical vapor deposition (MPCVD) reactor[11] which was modified[12] to allow swift gas exchange and continuous multilayer growth at a constant total pressure of 40 mbar. The injected microwave power of 280 W led to an estimated 910 °C temperature at the growing surface, which slightly depended on the composition of the gas phase. The process was the following: after 60 min in a pure hydrogen plasma allowing to stabilize the temperature and to remove any sp^2 contamination from the diamond substrate surface, a gas mixture of methane and oxygen diluted in hydrogen with a molar ratio equal to 0.75% for methane and 0.32% for oxygen was introduced at a total flow rate of 200 sccm in the reaction chamber, leading to the slow growth of the initial undoped buffer layer. Then, another gas mixture where a significant amount of diborane had been added to a 0.5% molar methane-in-hydrogen mixture was introduced at the same flow rate and pressure. This led to the growth (step 1) of p^+ diamond (diborane molar ratio to methane = 5000 ppm for samples SL1 and SL3, 4000 ppm for sample SL2), and

a)Author to whom correspondence should be addressed. Electronic mail: Etienne.bustarret@neel.cnrs.fr

resulted in solid state boron concentrations in the 2 to $8 \times 10^{20}\,cm^{-3}$ range.[12,13] This second mixture was flushed with pure hydrogen for 1 min (step 2) in order to ensure a sharp interface, before undertaking non intentionally doped (i) diamond homoepitaxial growth at a similar rate with a 1% molar methane mixture (step 3), and finally resuming the pure hydrogen flush step (step 4). Such a continuous p^+/i bilayer growth sequence was automatically repeated 20 times (17 times for SL3) without interrupting the plasma.

Multiwavelength ellipsometry was performed with a J.A. Woollam M2000 ellipsometer running under the Complete Ease software. The ellipsometric parameters (Ψ, Δ) and in particular the complex ratio $\boldsymbol{\rho}$ of the reflection coefficients for electric fields, respectively, parallel ($\mathbf{r_p}$) and perpendicular ($\mathbf{r_s}$) to the incidence plane ($\boldsymbol{\rho} = \mathbf{r_p}/\mathbf{r_s} = \tan(\Psi)\, e^{i\Delta}$) were monitored over the 210–1690 nm wavelength range at an incidence angle of 75° (*ex situ*) and 71° (*in situ*). The modulus of this complex ratio will be called hereafter the "polarization ratio." In the spirit of a previous publication,[9] both the *in situ* and *ex situ* ellipsometry spectra were simulated using a Cody-Lorentz model for the optical constants of diamond in the case of non-intentionally doped layers and by adding a Drude component to these UV oscillators for metallic p^+ layers. Contrary to the epitaxial layers, the 0.3–0.5 mm-thick diamond substrate was described as an "incoherent" optical layer, for which the intensities of the multiple reflected beams are summed, rather than their amplitudes.

As detailed elsewhere,[14] the offset of the ellipsometric parameter Δ resulting from the optical transmittance through the silica tube walls was estimated from the comparison of *in situ* and *ex situ* spectra of the same reference samples. We performed this calibration during the initial hydrogen plasma, as soon as the silica tube temperature became stable. The acquisition time for one spectrum was 1.5 s and the elapsed time between two consecutive measurements was 2.4 s. The samples were also characterized optically *ex situ* by normal incidence transmittance and oblique incidence reflectance spectroscopy over a 200–1000 nm wavelength range at low resolution (5 nm) in a Perkin-Elmer Lambda 900 double beam spectrophotometer.

High resolution X-ray diffraction (HRXRD) experiments were performed at the Cu $K_{\alpha 1}$ wavelength using a Seifert XRD 3003 PTS-HR diffractometer with a beam concentrator prior to the Ge(220) four-bounce monochromator and a Ge(220) double-bounce analyzer in front of the detector. The diffracted intensity profiles for the symmetric (004) reflection of diamond were simulated using the X'Pert Epitaxy software which relies on the dynamic theory of X-ray scattering and diffraction.[15] The variations of the electronic density and cell parameter of p^+ diamond with the boron concentration were deduced from linear Vegard-type laws based on previous first-principles calculations and diffraction experiments on thick p^+ epilayers.[16,17] The diffracted intensity was also mapped at high resolution around an asymmetric [−1–13] Bragg spot.

The initial variations of the polarization ratio measured *in situ* around 800 nm during the epitaxy of sample SL1, starting with the first p^+ layer homoepitaxially grown on the undoped diamond buffer layer, are presented in Fig. 1(a). The repetition over 20 cycles of the four-step sequence

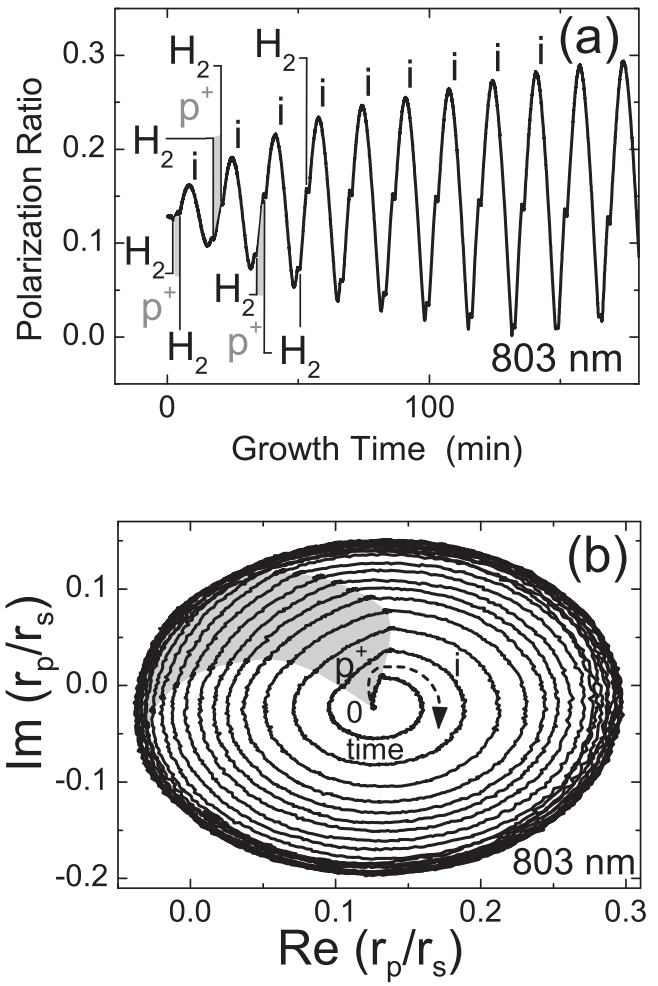

FIG. 1. *In situ* monitoring of the polarization ratio at 803 nm during the periodically alternated growth of p^+ and non intentionally doped i diamond, separated by short H_2 flushes, leading to sample SL1. The shaded areas indicate the first sectors corresponding to p^+ growth. (a) Time dependence of the polarization ratio during the first 11 cycles and (b) polar representation of the complex $\mathbf{r_p}/\mathbf{r_s}$ data collected at the same wavelength.

described above led to 20 oscillations governed by the ratio of the accumulated optical thickness to the monitoring wavelength. The amplitude of these oscillations increased with time, up to the 8th period where it reached a value of 0.25–0.3 which was maintained throughout the rest of the growth. Two small kinks per period may also be observed. These features correspond to the H_2 flush steps, where the layers not only stopped to grow but were slightly etched away.[12] The plot of the imaginary part of $\boldsymbol{\rho}$ as a function of its real part, with time as an implicit parameter, provided another illustration of the sensitivity of ellipsometry at a given wavelength to the doping level modulation. For the same set of ellipsometric parameters, this resulted in the spiral shown in Fig. 1(b), where the saturation effect after 8–10 periods is again quite striking. The kinks associated with H_2 flushes are also present on the left-hand side of this spiral, allowing a clear distinction between the sectors corresponding to the growth of non-intentionally doped i diamond and those monitoring p^+ diamond epitaxy. Actually, the monitoring wavelength has been chosen at 803 nm in order to maximize the amplitude of the oscillations. The area corresponding to p^+ sublayers epitaxy is smaller than that

attributed to i growth, indicating that quarter-wave conditions for each sublayer were not respected. Nevertheless, at this wavelength, a half-wave effect was expected and indeed observed for the full period under the angle of incidence of the optical set up (71°). This so-called half-wave effect describes the reflection peak observed at a wavelength equal to twice the optical thickness (for a given incidence) of one bilayer of the periodic multilayer. The building up of such a Bragg mirror effect as growth proceeds is illustrated by Fig. 2, where the polarization ratio spectra after 2, 7, 13 and 19 periods are presented. After seven cycles, the maximum amplitude at the peak wavelength was almost reached. Further cycling, even beyond the 13th period, had the main effect of reducing both the peak spectral width and the amplitude of the sidebands, while the peak wavelength became slightly lower.

Fitting parameters of the *ex situ* spectrum of sample SL1 taken in air at 75° incidence (Fig. 2) for the geometry (SL1 period = 187 nm, i thickness 152 nm, and p^+ thickness 35 nm) and Drude model (Doping level = $7 \times 10^{20}\,cm^{-3}$) were determined as described in a previous work.[9] Figure 3 shows the reflectance spectrum of sample SL1 measured at room temperature under a 12 ± 3° incidence. A 50% amplification of the reflectance with respect to the baseline (from 20% to 30%) was obtained at 833 nm. The reflectance peak of sample SL1 had a full width at half maximum (FWHM) of 60 nm, and was slightly asymmetrical (sharper at longer wavelengths). The transmittance spectrum (not shown here) presented a roughly 10% dip at 827 nm, superimposed with the slow decrease with wavelength typical of a free electron metal above the plasmon frequency.[7] A weaker second order Bragg peak can be seen around 420 nm.

Sample SL2 was designed for an effective half-wave effect occurring around the emission wavelength (638 nm) of the most popular[1–5] color center of diamond (NV^-), a region where both the refractive index contrast and the free carrier absorption are significantly lower than around 800 nm. The resulting reflectance spectrum is shown in Fig. 3 with a maximum in the expected range (640 nm). Fitting the *ex situ* ellipsometry spectrum of SL2 yielded a shorter period, 135 nm (20 nm p^+ and 115 nm i), and a lower doping level for the p^+ sublayer, around $3 \times 10^{20}\,cm^{-3}$. A lower index contrast was therefore expected, especially in the visible range. This feature is the first possible origin of the significantly weaker half-wave effect which was observed in sample SL2 when compared with SL1 (15% instead of 50%).

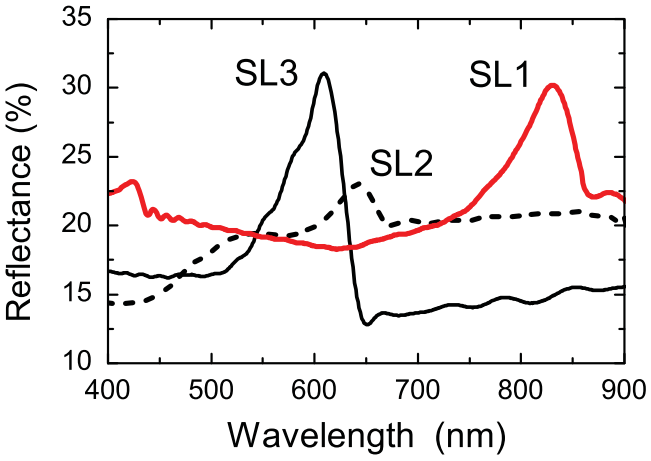

FIG. 3. Reflectance spectra of diamond doping superlattices SL1, SL2, and SL3 measured at room temperature under an angle of incidence of 12 ± 3°.

Another possible explanation would be a poorer quality of the doping transitions (sharpness and periodicity) in sample SL2. This hypothesis was tested performing X-ray diffraction measurements on samples SL1 and SL2. As can be seen on Fig. 4, a sharp (FWHM(2θ) = 0.013° = 230 μrad) peak was observed at a diffraction angle 2θ of 119.491° for the symmetrical reflection on the (004) planes of both the p^+ip^+i multilayer and (mainly) the diamond substrate. As expected for superlattices,[18] numerous satellite peaks were also present, their spacing being directly related to the period. This was determined from simulations to be 188 nm and 136 nm for samples SL1 and SL2, respectively, in good agreement with ellipsometry. The width and sharpness of

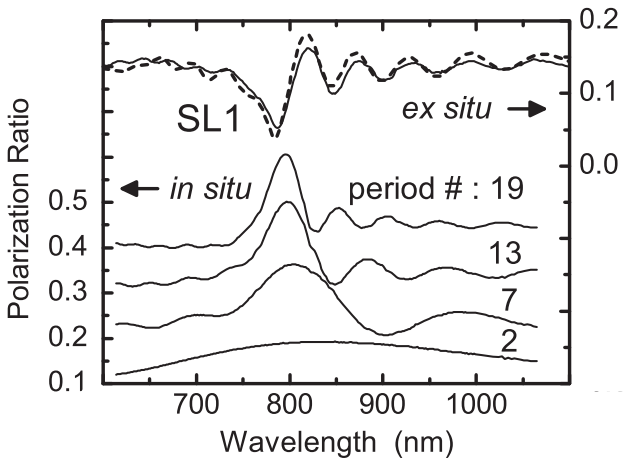

FIG. 2. Bottom, left-hand scale: polarization ratio spectra determined *in situ* by ellipsometry under a 71° incidence during the periodic growth of p^+/i bilayers after 2, 7, 13, and 19 epitaxial growth cycles for sample SL1. Top, right-hand scale: experimental (solid) and simulated (dashed) polarization ratio spectra of sample SL1 as measured *ex situ* at room temperature (angle of incidence: 75°).

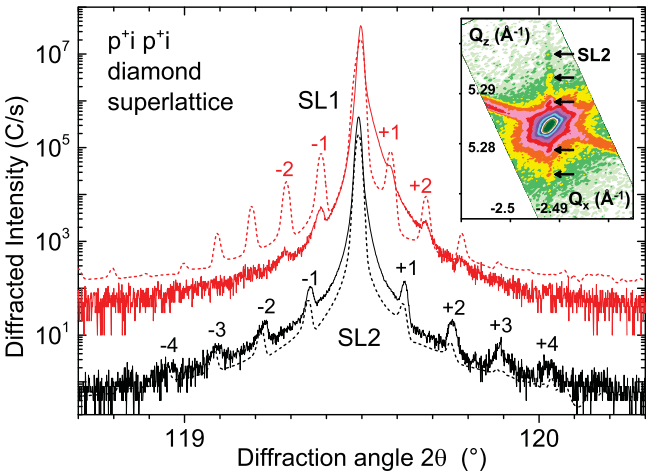

FIG. 4. Experimental (solid) and simulated (dashed) diffraction curves of two p^+ip^+i multilayers around the (004) symmetric reflection, with satellite peaks illustrating the superperiodicity of the epitaxial stacks. The curves have been vertically offset for clarity. The inset shows the diffraction intensity pattern around the asymmetric (–1–13) Bragg spot of the substrate measured on sample SL2.

these satellite peaks being related to the local variations of this period, their high number illustrates the small dispersion on the period. The four orders observed for SL2 illustrate the regularity of the automatic MPCVD cyclic process. Simulating the diffraction curves as shown in Fig. 4 yielded a total amount of boron (resp. 25 and $7 \times 10^{15}\,cm^{-2}$ for SL1 and SL2) in the superlattice. Assuming a rectangular doping profile, and thicknesses leading to simulated satellite intensities similar to those observed, this could correspond to average boron concentrations in the p^+ layer around $4 \times 10^{20}\,cm^{-3}$ for a 35 nm-thick p^+ sublayer in the case of SL1 and $2 \times 10^{20}\,cm^{-3}$ in a 20 nm-thick p^+ sublayer for SL2.

The inset of Fig. 4 shows the iso-intensity contours in the reciprocal space for the asymmetric diffraction from the (−1–13) planes of sample SL2. Beside the strong spot (substrate) and the oblique high intensity line, illustrating the angular resolution of the system, there is a fainter vertical line with vertically spaced intensity peaks resulting from the super-periodicity of the system. The central location of this line confirms that the whole system has the same in-plane lattice parameter, so that all doped epilayers are fully strained in the surface plane, while the out-of-plane lattice parameter becomes slightly larger in the p^+ epilayers as documented by numerous previous works.[8,16,17] The verticality and narrowness of this line illustrate the high crystalline quality of the superlattice and the low level of short range disorder. This was confirmed by the FWHM of the rocking curve (40 μrad) of the −1 satellite peak being narrower than that of the substrate, suggesting that the structural quality has been improved in the epilayers with respect to the substrate. As seen in Fig. 4, the (004) diffraction curve for SL1 yields a lower number of satellites, which are slightly closer to each other, confirming the longer and probably less perfect periodicity of this superlattice. Therefore, the difference in amplitude of the reflectance Bragg peak between both samples cannot be explained by a poorer quality of SL2.

A third possible cause for the weaker peak reflectance of sample SL2 is that the thickness of the p^+ layer (20 nm, i.e., 15% of the period) was too low: For non-absorbing layers, it is well known that the efficiency of a Bragg mirror may be increased by tuning the optical thickness of each individual sublayer of the superlattice to a quarter of the target wavelength. This was not the case in sample SL2. In the case where one of the two layers is not completely transparent (here p^+), a trade-off has to be found between the optimal double quarter wave situation and the losses associated with the absorption in the p^+ material. Simulations indicated that using the doping level of SL1 and increasing the relative thickness of the p^+ sublayer should increase the reflectance contrast. A third superlattice (SL3) was grown with these characteristics repeated over 17 cycles. *Ex situ* ellipsometry indicated that its period was 139 nm (54 nm for i and 85 nm for p^+). The resulting reflectance spectrum, shown in Fig. 3, yielded a Bragg peak very similar to that of SL1, with a factor two amplification (100% instead of 50%), but at 610 nm. The peak wavelength could be shifted to 580 nm at 45° incidence, matching fairly well the room temperature emission of the NV^0 center. Attention should be paid to the fact that the refraction was affected by the finite extinction coefficient: The apparent refractive index became lower than the real part of the complex index.[19,20] This effect induced a better index contrast between the two layers, and caused also more absorption along the multilayer Bragg stack, leading us to reduce the number of periods from 20 to 17. Finally, sample SL3 was strongly absorbing, so that its "background" reflectance value in the visible range was 15%, significantly weaker than that of the two previous superlattices (see Fig. 3), and only slightly stronger than that of a thick p^+ material.[7,8] With a Bragg peak maximum at 30%, this contributed to the enhancement of the mirror efficiency and wavelength selectivity. Furthermore, the sharper reflectance drop on the long wavelength side of the peak was found well suited to cutting off the broad phonon related side bands from the sharper zero phonon line emission of NV centers.

Although further optimization is still required to tune the quarter wave effect to the wavelengths of $NV^-$and SiV^- centers, we believe that the present results demonstrate without ambiguity the practical potential of modulating the doping level over periodic stacks of diamond homoepitaxial layers for fabricating all-diamond monolithic Bragg mirrors, opening the way to optical cavities containing diamond color centers.

[1]B. J. M. Hausmann, M. Khan, Y. Zhang, T. M. Babinec, K. Martinick, M. McCutcheon, P. R. Hemmer, and M. Lončar, Diamond Relat. Mater. **19**, 621 (2010).
[2]T. M. Babinec, B. J. M. Hausmann, M. Khan, Y. Zhang, J. R. Maze, P. R. Hemmer, and M. Lončar, Nat. Nanotechnol. **5**, 195 (2010).
[3]E. Neu, P. Appel, M. Ganzhorn, J. Miguel-Sanchez, M. Lesik, V. Mille, V. Jacques, A. Tallaire, J. Achard, and P. Maletinsky, Appl. Phys. Lett. **104**, 153108 (2014).
[4]H. Berbien, L. Childress, L. Robledo, M. Markham, D. Twitchen, and R. Hanson, Phys. Rev. Lett. **108**, 043604 (2012).
[5]C. Hepp, T. Müller, V. Waselowski, J. N. Becker, B. Pingault, H. Sternschulte, D. Steinmüller-Nethl, A. Gali, J. R. Maze, M. Atatüre, and C. Becher, Phys. Rev. Lett. **112**, 036405 (2014).
[6]P. Olivero, S. Rubanov, P. Reichart, B. C. Gibson, S. T. Huntington, J. Rabeau, A. D. Greentree, J. Salzman, D. Moore, D. N. Jamieson, and S. Prawer, Adv. Mater. **17**, 2427 (2005).
[7]E. Bustarret, F. Pruvost, M. Bernard, and C. Uzan-Saguy, Phys. Status Solidi A **186**, 303 (2001).
[8]E. Bustarret, E. Gheeraert, and K. Watanabe, Phys. Status Solidi A **199**, 9 (2003).
[9]J. Bousquet, G. Chicot, D. Eon, and E. Bustarret, Appl. Phys. Lett. **104**, 021905 (2014).
[10]M. H. Nazaré, A. J. Neves, and G. Davies, Phys. Rev. B **43**, 14196 (1991).
[11]M. Kamo, Y. Sato, S. Matsumoto, and N. Setaka, J. Cryst. Growth **62**, 642 (1983).
[12]A. Fiori, T. N. Tran Thi, G. Chicot, F. Jomard, F. Omnès, E. Gheeraert, and E. Bustarret, Diamond Relat. Mater. **24**, 175 (2012).
[13]G. Chicot, T. N. Tran Thi, A. Fiori, F. Jomard, E. Gheeraert, E. Bustarret, and J. Pernot, Appl. Phys. Lett. **101**, 162101 (2012).
[14]J. Bousquet, F. Jomard, E. Bustarret, and D. Eon (unpublished results).
[15]D. K. Bowen and B. K. Tanner, *High Resolution X-ray diffraction and Topography* (Taylor and Francis Ltd, London, 1998).
[16]T. Wojewoda, P. Achatz, L. Ortéga, F. Omnès, C. Marcenat, E. Bourgeois, X. Blase, F. Jomard, and E. Bustarret, Diamond Relat. Mater. **17**, 1302 (2008).
[17]B. Guzman de la Mata, A. Sanz-Hervás, M. G. Dowsett, M. Schwitters, and D. Twitchen, Diamond Relat. Mater. **16**, 809 (2007).
[18]Y. Kotsar, P. K. Kandaswamy, A. Das, E. Sarigiannidou, E. Bellet-Amalric, and E. Monroy, J. Cryst. Growth **323**, 64 (2011).
[19]M. A. Dupertuis, M. Proctor, and B. Acklin, J. Opt. Soc. Am. A **11**, 1159 (1994).
[20]P. C. Y. Chang, J. G. Walker, and K. I. Hopcraft, J. Quant. Spectrosc. Radiat. Transfer **96**, 327 (2005).